

Lattice Boltzmann approach to rarefied gas flows using half-range Gauss-Hermite quadratures: Comparison to DSMC results based on ab initio potentials

Victor E. Ambruş,^{1,*} Felix Sharipov,^{2,†} and Victor Sofonea^{3,‡}

¹*Department of Physics, West University of Timișoara,
Bd. Vasile Pârvan 4, Timișoara 300223, Romania*

²*Departamento de Física, Universidade Federal do Paraná, Curitiba, 81531-980 Brazil*

³*Center for Fundamental and Advanced Technical Research, Romanian Academy,
Bd. Mihai Viteazul 24, Timișoara 300223, Romania*

In this paper, we employ the lattice Boltzmann method to solve the Boltzmann equation with the Shakhov model for the collision integral in the context of the 3D planar Couette flow. The half-range Gauss-Hermite quadrature is used to account for the wall-induced discontinuity in the distribution function. The lattice Boltzmann simulation results are compared with direct simulation Monte Carlo (DSMC) results for ^3He and ^4He atoms interacting via ab initio potentials, at various values of the rarefaction parameter δ , where the temperature of the plates varies from 1 K up to 3000 K. Good agreement is observed between the results obtained using the Shakhov model and the DSMC data at large values of the rarefaction parameter. The agreement deteriorates as the rarefaction parameter is decreased, however we highlight that the relative errors in the non-diagonal component of the shear stress do not exceed 2.5%.

arXiv:1810.07803v2 [physics.comp-ph] 13 Mar 2019

* E-mail: victor.ambrus@e-uvt.ro

† E-mail: sharipov@fisica.ufpr.br

‡ E-mail: sofonea@gmail.com; Corresponding author.

I. INTRODUCTION

The main difficulty in simulating steady-state rarefied channel flows is caused by the discontinuity in the distribution function induced by the particle-wall interaction. A generally accepted method for the simulation of rarefied flows is the Direct Simulation Monte Carlo (DSMC) method. Although accurate, DSMC simulations are computationally demanding, particularly in the hydrodynamic and transition regimes. A convenient alternative to DSMC is the Boltzmann equation with a suitable model (e.g., BGK [1] or Shakhov [2]) for the collision term [3]. Various numerical methods have been developed to solve such model equations, including the Discrete Velocity Method (DVM) [3], the Discrete Unified Gas Kinetic Scheme (DUGKS) [4], the discrete Boltzmann models [5] and the lattice Boltzmann (LB) models [6].

Close to the hydrodynamic regime, reliable results can be obtained using lattice Boltzmann models based on the D3Q27 model [7], the spherical decomposition of the velocity space [8] or the full-range Gauss-Hermite quadrature [6, 9]. As the degree of rarefaction increases, the number of velocities required by such models to ensure accurate results increases significantly [6, 8, 10, 11]. This is due to the discontinuity of the distribution function, which develops due to the particle-wall interaction [12, 13]. When the gas is far from equilibrium, this discontinuity can be managed more efficiently with LB models based on half-range Gauss-Hermite quadratures. As demonstrated in the context of the Couette flow between parallel plates [6, 11], the ratio between the number of velocities used when full-range or half-range Gauss-Hermite quadratures are employed on the Cartesian axis perpendicular to the wall increases dramatically for values of the Knudsen number Kn exceeding 0.1 (e.g., at $\text{Kn} = 0.5$, this ratio is 9.5).

In this contribution, we validate our LB simulation results by comparison to the DSMC results reported in Ref. [14], which were obtained for dilute gases comprised of ^3He and ^4He atoms that interact via quantum scattering cross-sections, computed using ab initio potentials. The connection between the Shakhov model employed in the LB method and the interaction model employed in the DSMC method is made by implementing the relaxation time τ and the Prandtl number Pr such that the viscosity μ and heat conductivity κ match the values computed in Ref. [15].

The paper is structured as follows. First, the application of the Shakhov model with reduced distributions for the simulation of gases with interparticle interactions based on ab initio potentials is discussed. Next, we introduce the mixed quadrature LB models, which employ the half-range Gauss-Hermite quadrature on the axis perpendicular to the wall. The comparison of the numerical results obtained using the Shakhov collision model and the full DSMC analysis is further discussed. Finally, we present our conclusions.

II. SHAKHOV KINETIC MODEL FOR THE COUETTE FLOW

In this paper, we focus on the study of the Couette flow between parallel plates. The coordinate system is chosen such that the x axis is perpendicular to the walls. The origin of the coordinate system is taken to be on the channel centerline, such that the left and right walls are located at $x = -L/2$ and $x = L/2$, respectively. The plates are set in motion along the y axis and the flow is studied in the Galilean frame where the left and right plates move with velocities $-u_w$ and u_w , respectively. Both plates are kept at constant temperature T_w . In this case, the Boltzmann equation with the Shakhov approximation for the collision term can be written as follows [2, 8, 16]:

$$\frac{\partial f}{\partial t} + \frac{p_x}{m} \partial_x f = -\frac{1}{\tau} \left[f - f^{(\text{eq})} (1 + \mathbb{S}) \right], \quad (2.1)$$

where f is the particle distribution function, p_x is the particle momentum along the direction perpendicular to the walls, m is the particle mass and τ is the relaxation time. The Maxwell-Boltzmann distribution function $f^{(\text{eq})}$ for the ideal gas is:

$$f^{(\text{eq})} = n g(p_x, u_x, T) g(p_y, u_y, T) g(p_z, u_z, T), \quad g(p, u, T) = \frac{1}{\sqrt{2\pi m K_B T}} e^{-(p-mu)^2/2mK_B T}, \quad (2.2)$$

where u_α is the macroscopic velocity along the α direction ($\alpha \in \{x, y, z\}$), while n and T are the particle number density and the local temperature, respectively. The Shakhov term \mathbb{S} is given by:

$$\mathbb{S} = \frac{1 - \text{Pr}}{n K_B^2 T^2} \left(\frac{\xi^2}{5m K_B T} - 1 \right) \mathbf{q} \cdot \boldsymbol{\xi}, \quad (2.3)$$

where $\xi_\alpha = p_\alpha - m u_\alpha$ and q_α are the α components of the peculiar velocity and heat flux vectors. The Prandtl number $\text{Pr} = c_p \mu / \kappa$, where $c_p = 5K_B/2m$, represents a free parameter of the Shakhov model. This parameter can be used to tune the heat conductivity κ , while the viscosity is proportional to the relaxation time τ and is given by $\mu = \tau P$, where $P = n K_B T$ is the ideal gas pressure.

Since the flow properties are trivial along the z direction, it is convenient to introduce the reduced distributions ϕ and χ through [17, 18]:

$$\phi = \int_{-\infty}^{\infty} dp_z f, \quad \chi = \int_{-\infty}^{\infty} dp_z \frac{p_z^2}{m} f. \quad (2.4)$$

The equations obeyed by the reduced distributions ϕ and χ can be obtained by multiplying Eq. (2.1) with 1 and p_z^2/m and integrating over p_z :

$$\frac{\partial}{\partial t} \begin{pmatrix} \phi \\ \chi \end{pmatrix} + \frac{p_x}{m} \frac{\partial}{\partial x} \begin{pmatrix} \phi \\ \chi \end{pmatrix} = -\frac{1}{\tau} \begin{bmatrix} \phi - \phi^{(\text{eq})}(1 + \mathbb{S}_\phi) \\ \chi - \chi^{(\text{eq})}(1 + \mathbb{S}_\chi) \end{bmatrix}, \quad (2.5)$$

where $\phi^{(\text{eq})} = ng(p_x, u_x, T)g(p_y, u_y, T)$, $\chi^{(\text{eq})} = K_B T \phi^{(\text{eq})}$ and the Shakhov terms \mathbb{S}_ϕ and \mathbb{S}_χ are given by:

$$\mathbb{S}_\phi = \frac{1 - \text{Pr}}{nK_B^2 T^2} \left(\frac{\xi_x^2 + \xi_y^2}{5mK_B T} - \frac{4}{5} \right) (q_x \xi_x + q_y \xi_y), \quad \mathbb{S}_\chi = \frac{1 - \text{Pr}}{nK_B^2 T^2} \left(\frac{\xi_x^2 + \xi_y^2}{5mK_B T} - \frac{2}{5} \right) (q_x \xi_x + q_y \xi_y). \quad (2.6)$$

The macroscopic quantities describing the fluid can be obtained as moments of ϕ and χ , as follows:

$$\begin{pmatrix} n \\ u_i \\ T_{ij} \end{pmatrix} = \int dp_x dp_y \begin{pmatrix} 1 \\ p_i/\rho \\ \xi_i \xi_j/m \end{pmatrix} \phi, \quad T_{zz} = \int dp_x dp_y \chi, \quad (2.7)$$

$$\begin{pmatrix} q_x \\ q_y \end{pmatrix} = \int dp_x dp_y \left[\begin{pmatrix} (\xi_x^2 + \xi_y^2)\xi_x/2m^2 \\ (\xi_x^2 + \xi_y^2)\xi_y/2m^2 \end{pmatrix} \phi + \begin{pmatrix} \xi_x/2m \\ \xi_y/2m \end{pmatrix} \chi \right], \quad (2.8)$$

where i, j take values in $\{x, y\}$, while $u_z = T_{xz} = T_{yz} = q_z = 0$. The temperature is obtained via $T = \frac{1}{3nK_B}(T_{xx} + T_{yy} + T_{zz})$.

Due to the symmetries of Eq. (2.5), $\phi(-x, -p_x, -p_y) = \phi(x, p_x, p_y)$ and $\chi(-x, -p_x, -p_y) = \chi(x, p_x, p_y)$ for $0 \leq x \leq L/2$, such that only the right half of the channel can be considered. At $x = L/2$, diffuse reflection boundary conditions are imposed:

$$\begin{aligned} \phi(x = L/2, p_x < 0) &= n_w g(p_x, 0, T_w) g(p_y, u_w, T_w), \\ \chi(x = L/2, p_x < 0) &= n_w K_B T_w g(p_x, 0, T_w) g(p_y, u_w, T_w), \end{aligned} \quad (2.9)$$

where n_w is obtained by imposing zero mass flux through the wall:

$$n_w = -\frac{\int_0^\infty dp_x \int_{-\infty}^\infty dp_y \phi(x = L/2) p_x}{\int_{-\infty}^0 dp_x \int_{-\infty}^\infty dp_y g(p_x, 0, T_w) g(p_y, u_w, T_w) p_x}. \quad (2.10)$$

The connection between the relaxation time approximation of the Boltzmann equation and the full collision integral for a given interaction model can be made at the level of the transport coefficients. For simple interaction models such as the hard-sphere or Maxwell molecules gases, the viscosity has a temperature dependence of the form

$$\mu = \mu_{\text{ref}}(T/T_{\text{ref}})^\omega, \quad (2.11)$$

where the viscosity index ω takes the values 1/2 and 1 for hard sphere and Maxwell molecules, respectively. For real gases, ω is in general temperature-dependent. In the context of interactions based on ab initio potentials, the viscosity μ was tabulated for gases comprised of ^3He and ^4He atoms in the supplementary materials of Ref. [15]. In this work, we employ Eq. (2.11) in a piecewise fashion by determining appropriate values of ω in order to interpolate the tabulated data, as follows. Considering that the data table contains N entries, let μ_n and μ_{n+1} ($1 \leq n < N$) represent two consecutive values of the viscosity, corresponding to the values T_n and T_{n+1} of the temperature. For the interval $T \in [T_n, T_{n+1}]$, Eq. (2.11) is replaced by:

$$\mu^{(n)}(T) = \mu_n (T/T_n)^{\omega_n}, \quad \omega_n = \frac{\ln(\mu_{n+1}/\mu_n)}{\ln(T_{n+1}/T_n)}, \quad (2.12)$$

such that $\mu^{(n)}(T_n) = \mu_n$ and $\mu^{(n)}(T_{n+1}) = \mu_{n+1}$. We also take advantage of the freedom in controlling the Prandtl number Pr via the Shakhov collision model in order to track the (small) variations of Pr with temperature. For simplicity, we consider a piecewise constant implementation of Pr , such that $\text{Pr} = \text{Pr}_n$ when $T_n \leq T < T_{n+1}$, where

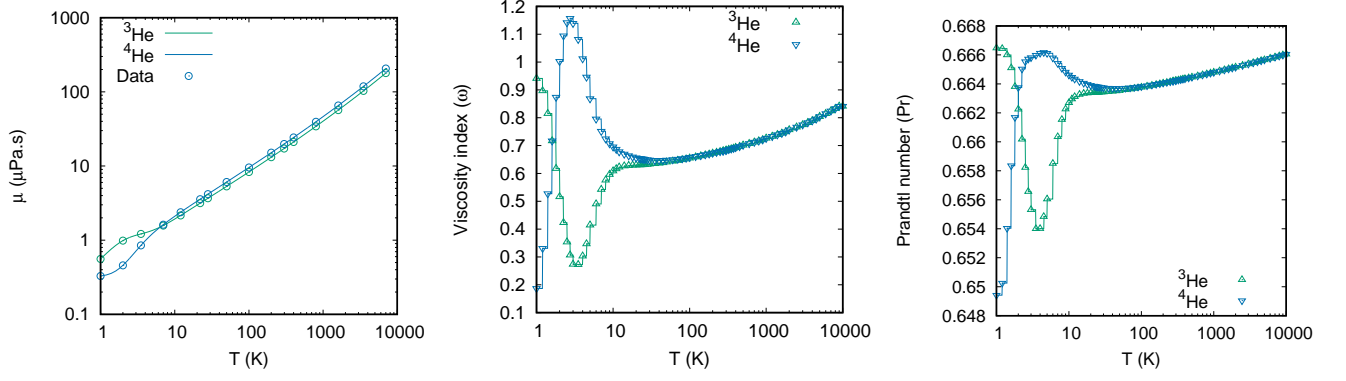


FIG. 1. Temperature dependence of (a) dynamic viscosity μ (in $\mu\text{Pa} \cdot \text{s}$); (b) viscosity index ω ; and (c) Prandtl number Pr , as given by Eqs. (2.12) and (2.13). In (a), the tabulated values [15] for the viscosity are shown using hollow circles, while the continuous lines correspond to the piecewise functions defined in Eq. (2.12). The viscosity index and Prandtl number are shown as piecewise constant functions, while the symbols mark the values obtained via the tabulated data from Ref. [15].

$\text{Pr}_n = c_p \mu_n / \kappa_n$ is obtained using the tabulated value κ_n of the heat conductivity corresponding to $T = T_n$. In order to access temperature ranges outside the tabulated data, Eq. (2.11) is extrapolated by taking $\mu(T) = \mu^{(1)}(T)$ and $\text{Pr}(T) = \text{Pr}_1$ for $T < T_2$, while $\mu(T) = \mu^{(N-1)}(T)$ and $\text{Pr}(T) = \text{Pr}_N$ for $T > T_N$. The mathematical expression for the above algorithm is:

$$\mu(T) = \begin{cases} \mu^{(1)}(T), & T < T_2, \\ \mu^{(n)}(T), & T_n < T < T_{n+1}, \\ \mu^{(N-1)}(T), & T_N < T, \end{cases} \quad \text{Pr}(T) = \begin{cases} \text{Pr}_1, & T < T_2, \\ \text{Pr}_n, & T_n < T < T_{n+1}, \\ \text{Pr}_N, & T_N < T, \end{cases} \quad (2.13)$$

where $n = 2, 3, \dots, N-1$ refers to the index of the tabulated values in Ref. [15]. The interpolation corresponding to Eq. (2.13) is shown in Fig. 1, where the viscosity $\mu(T)$ is shown as a continuous function, while the viscosity index ω and the Prandtl number Pr are shown as piecewise functions. It can be seen that while Pr is confined within a few percent of the expected value $2/3$, the viscosity index presents significant variations, especially in the low temperature regime.

The degree of rarefaction of the flow can be described using the rarefaction parameter δ , defined through [14]:

$$\delta = \frac{LP_{\text{ref}}}{\mu(T_w)v_{\text{ref}}\sqrt{2}}, \quad (2.14)$$

where $P_{\text{ref}} = n_{\text{ref}}K_B T_w$, n_{ref} is the average particle number density and $v_{\text{ref}} = \sqrt{K_B T_w / m}$ is the reference speed. The relaxation time can thus be written in terms of the rarefaction parameter as follows:

$$\tau = \frac{\mu(T)/\mu(T_w)}{(n/n_{\text{ref}})(T/T_w)} \frac{t_{\text{ref}}}{\delta\sqrt{2}}, \quad (2.15)$$

where the reference time is $t_{\text{ref}} = L/v_{\text{ref}}$.

III. MIXED QUADRATURE LATTICE BOLTZMANN MODELS

In this section, the LB algorithm employed to solve Eq. (2.5) is briefly described. Our implementation is based on the concept of mixed quadratures [6, 11, 19], which allows the quadrature to be controlled on each axis independently (more details on the concept of Gaussian quadrature can be found in, e.g., Refs. [20, 21]). In particular, the half-range Gauss-Hermite quadrature is employed on the x axis, where the distribution function becomes discontinuous due to the diffuse reflection boundary conditions [12, 13]. On the periodic (y) direction, the full-range Gauss-Hermite quadrature is employed since there are no discontinuities of the distribution function with respect to p_y . The technical details regarding the construction of such models are given in Ref. [6] in the context of the 2D Couette flow and the application of these models to the 3D Couette flow using reduced distributions is discussed in Ref. [16]. In this section, the main ingredients necessary to employ these models are summarized.

The half-range Gauss-Hermite quadrature allows the recovery of the integrals with respect to p_x on each semi-axis individually, as follows:

$$\int_0^\infty \frac{dp_x}{\sqrt{2\pi}} e^{-p_x^2/2p_{0,x}^2} p_x^s \simeq p_{0,x} \sum_{i=1}^{Q_x} w_i^h p_{x,i}^s, \quad \int_{-\infty}^0 \frac{dp_x}{\sqrt{2\pi}} e^{-p_x^2/2p_{0,x}^2} p_x^s \simeq p_{0,x} \sum_{i=1}^{Q_x} w_i^h (-p_{x,i})^s, \quad (3.1)$$

where equality holds when $2Q_x > s$. The ratios between the discrete momentum values $p_{x,i}$ ($1 \leq i \leq Q_x$) and the arbitrary reference momentum scale $p_{0,x}$ are the roots of the half-range Hermite polynomial $\mathfrak{h}_{Q_x}(z)$, of order Q_x [i.e. $\mathfrak{h}_{Q_x}(p_{x,i}/p_{0,x}) = 0$]. The quadrature weight corresponding to the quadrature point $p_{x,i}/p_{0,x}$ is obtained through [6]:

$$w_i^{\mathfrak{h}} = \frac{p_{x,i} a_{Q_x-1}^2}{\mathfrak{h}_{Q_x-1}^2(p_{x,i}/p_{0,x}) [p_{x,i} + p_{0,x} \mathfrak{h}_{Q_x}^2(0)/\sqrt{2\pi}]}, \quad (3.2)$$

where $a_\ell = \mathfrak{h}_{\ell+1, \ell+1}/\mathfrak{h}_{\ell, \ell}$ and $\mathfrak{h}_{\ell, s}$ is the coefficient of z^s in $\mathfrak{h}_\ell(z)$. We use the convention that $p_{x,i+Q_x} = -p_{x,i}$, such that $w_{x,i+Q_x}^{\mathfrak{h}} = w_{x,i}^{\mathfrak{h}}$.

The integrals with respect to p_y can be recovered using the full-range Gauss-Hermite quadrature, as follows:

$$\int_{-\infty}^{\infty} \frac{dp_y}{\sqrt{2\pi}} e^{-p_y^2/2p_{0,y}^2} p_y^s \simeq p_{0,y} \sum_{j=1}^{Q_y} w_j^H p_{y,j}^s, \quad (3.3)$$

where equality is achieved when the quadrature order Q_y satisfies $2Q_y > s$. The ratios $p_{y,j}/p_{0,y}$ are the roots of the full-range Hermite polynomial $H_{Q_y}(z)$ of order Q_y , i.e. $H_{Q_y}(p_{y,j}/p_{0,y}) = 0$, where $p_{0,y}$ is an arbitrary reference momentum scale. The quadrature weights w_j^H can be computed using [6]:

$$w_j^H = \frac{Q_y!}{H_{Q_y+1}^2(p_{y,j}/p_{0,y})}. \quad (3.4)$$

After the discretization of the momentum space, the factors $g(p_x, u_x, T)$ and $g(p_y, u_y, T)$ in Eq. (2.2) are replaced by a set of polynomial truncations $g_{x,i}(u_x, T)$ and $g_{y,j}(u_y, T)$ of orders $0 \leq N_x < Q_x$ and $0 \leq N_y < Q_y$ with respect to the half-range and the full-range Hermite polynomials, respectively. In particular, $g(p_x, u_x, T)$ is replaced by

$$g_{x,i} = \frac{w_i^{\mathfrak{h}} \sqrt{2\pi}}{e^{-p_{x,i}^2/2p_{0,x}^2}} g(p_{x,i}, u_x, T) = \frac{w_i^{\mathfrak{h}}}{2} \sum_{s=0}^{N_x} \left(\frac{mK_B T}{2p_{0,x}^2} \right)^{\frac{s}{2}} \left[(1 + \operatorname{erf} \zeta_{x,i}) P_s^+(\zeta_{x,i}) + \frac{2e^{-\zeta_{x,i}^2}}{\sqrt{\pi}} P_s^*(\zeta_{x,i}) \right] \Phi_{s,i}^{N_x}, \quad (3.5)$$

where $1 \leq i \leq 2Q_x$, $\zeta_{x,i} = \sigma_{x,i} u_x \sqrt{m/2K_B T}$, $\sigma_{x,i}$ is the sign of $p_{x,i}$, $\Phi_{s,i}^{N_x} = \sum_{\ell=s}^{N_x} \mathfrak{h}_{\ell,s} \mathfrak{h}_\ell(|p_{x,i}/p_{0,x}|)$ and the polynomials $P_s^+(\zeta)$ and $P_s^*(\zeta)$ are given by:

$$P_s^\pm(\zeta) = e^{\mp \zeta^2} \frac{d^s}{d\zeta^s} e^{\pm \zeta^2}, \quad P_s^*(\zeta) = \sum_{j=0}^{s-1} \binom{s}{j} P_j^+(\zeta) P_{s-j-1}^-(\zeta). \quad (3.6)$$

Similarly, $g(p_y, u_y, T)$ is replaced by:

$$g_{y,j} = \frac{w_j^H \sqrt{2\pi}}{e^{-p_{y,j}^2/2p_{0,y}^2}} g(p_{y,j}, u_y, T) = w_j^H \sum_{\ell=0}^{N_y} H_\ell(p_{y,j}) \sum_{s=0}^{\lfloor \ell/2 \rfloor} \frac{1}{2^s s! (\ell - 2s)!} \left(\frac{mK_B T}{p_{0,y}^2} - 1 \right)^s \left(\frac{m u_y}{p_{0,y}} \right)^{\ell - 2s}, \quad (3.7)$$

where $1 \leq j \leq Q_y$. The polynomial truncations (3.5) and (3.7) are constructed such that the half-space and full-space moments of $g(p_x, u_x, T)$ and $g(p_y, u_y, T)$, respectively, are exactly recovered via the following quadrature sums [6, 11]:

$$\int_0^\infty dp_x g(p_x, u_x, T) p_x^s = \sum_{i=1}^{Q_x} g_{x,i} p_{x,i}^s, \quad \int_{-\infty}^0 dp_x g(p_x, u_x, T) p_x^s = \sum_{i=Q_x+1}^{2Q_x} g_{x,i} p_{x,i}^s, \\ \int_{-\infty}^\infty dp_y g(p_y, u_y, T) p_y^\ell = \sum_{j=1}^{Q_y} g_{y,j} p_{y,j}^\ell, \quad (3.8)$$

for all values of s and ℓ which satisfy $0 \leq s \leq N_x$ and $0 \leq \ell \leq N_y$.

The resulting mixed quadrature LB models are denoted through $\text{HHLB}(N_x; Q_x) \times \text{HLB}(N_y; Q_y)$, where N_x and N_y are the expansion orders of the equilibrium distribution and Q_x and Q_y are the quadrature orders of the half-range and full-range Gauss-Hermite quadratures.

The solution of Eq. (2.5) is obtained using the total variation diminishing (TVD) third order Runge-Kutta (RK-3) integration method introduced in Ref. [22] together with the fifth order weighted essentially non-oscillatory (WENO-5) advection scheme introduced in Ref. [23]. In order to accurately capture the Knudsen layer in the vicinity of the wall

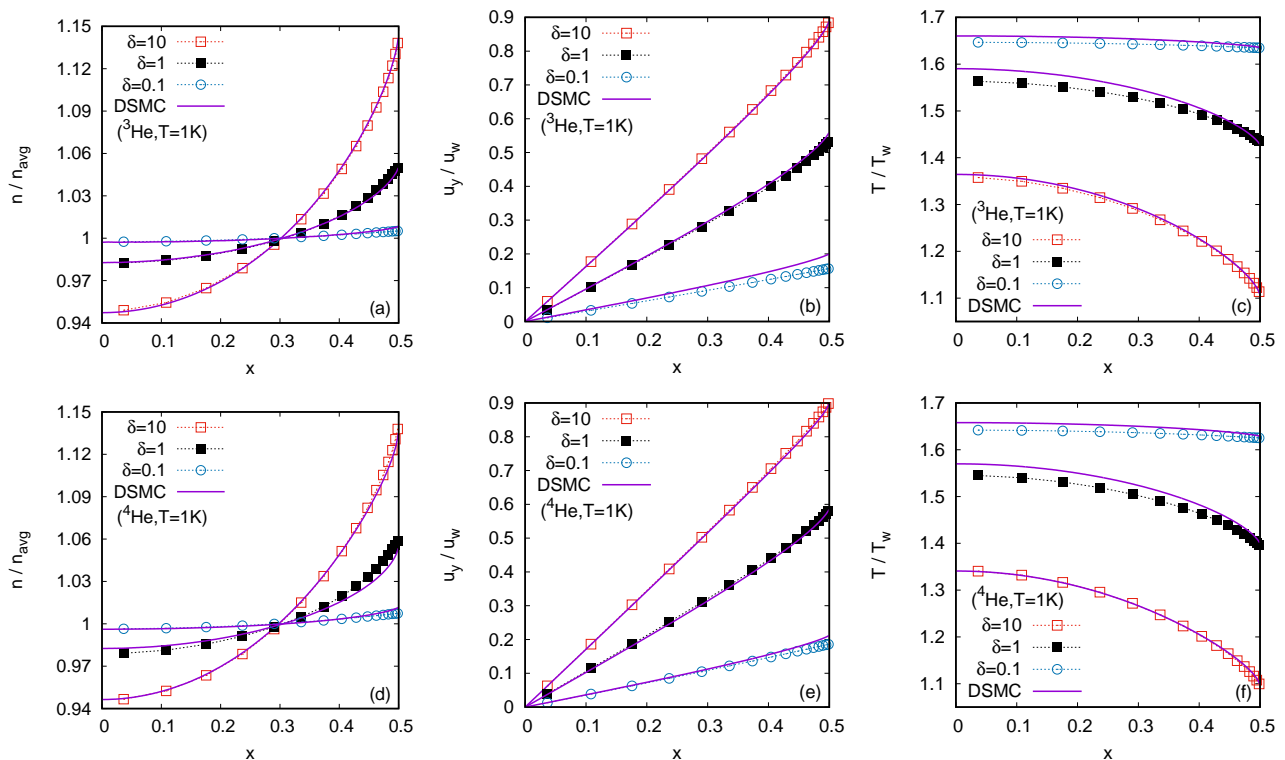


FIG. 2. Comparison between the LB (dotted lines and points) and DSMC (continuous lines) results for the profiles of n (left), u_y (middle) and T (right) through half of the channel ($0 \leq x \leq L/2$), for ${}^3\text{He}$ (top) and ${}^4\text{He}$ (bottom) gas constituents. The wall temperature is set to $T_w = 1$ K and the wall velocity is $u_w = \sqrt{2K_B T_w/m}$.

at $x = L/2$, a coordinate stretching procedure is employed following Ref. [24], which is given through the following coordinate transformation [16, 25]:

$$x(\eta) = \frac{L}{2A} \tanh \eta. \quad (3.9)$$

The stretching parameter A takes values between 0 and 1, while the domain for η is $0 \leq \eta \leq \text{arctanh } A$. The discretization of the flow domain is performed using S equidistant values for η , namely $\eta_s = \frac{1}{S}(s - 1/2)\text{arctanh } A$ ($1 \leq s \leq S$). This allows the advection scheme to be implemented using a finite difference formulation, as described in Refs. [16, 25]. For simplicity, we only consider the case when $A = 0.98$ in the simulations presented in the following sections.

IV. NUMERICAL RESULTS

In order to compare the DSMC and LB methods considered in this paper, we performed simulations for gases comprised of ${}^3\text{He}$ and ${}^4\text{He}$ atoms, for wall temperatures varying between 1 K and 3000 K. The numerical scheme of the DSMC method used in the present work is described in Ref. [14]. The wall velocity is set to $u_w = \sqrt{2K_B T_w/m}$. Three values of the rarefaction parameter δ were used, namely $\delta \in \{10, 1, 0.1\}$. The number of nodes was always kept at $S = 16$ and the quadrature orders employed are discussed at the end of this section.

Figures 2 and 3 show a comparison of the LB and DSMC results for $T_w = 1$ K and 300 K at the level of the profiles of n , u_y and T , for both the ${}^3\text{He}$ and the ${}^4\text{He}$ gases. Good agreement can be seen at $\delta = 10$, while at $\delta = 0.1$, there are some discrepancies between the results for u_y and T . The discrepancy in the temperature profile persists also at $\delta = 1$.

We next consider a comparison of the LB and DSMC results for the off-diagonal component of the stress tensor T_{xy} , which we present through the non-dimensional number

$$\Pi = -\frac{T_{xy}v_{\text{ref}}}{P_{\text{ref}}u_w\sqrt{2}}. \quad (4.1)$$

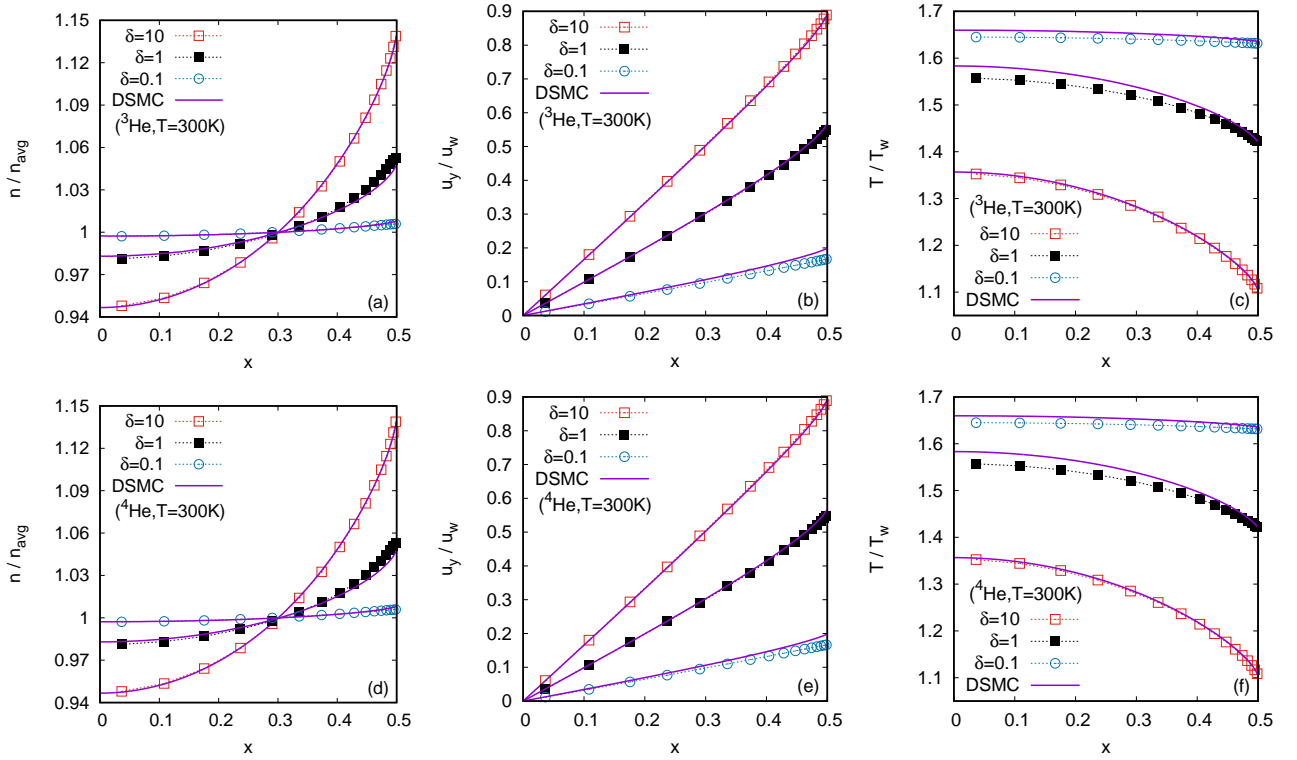


FIG. 3. The same as in Fig. 2, but with wall temperature $T_w = 300$ K.

Noting that $u_w = \sqrt{2K_B T_w / m} = v_{\text{ref}} \sqrt{2}$, it can be seen that $\Pi = -T_{xy} / 2P_{\text{ref}}$. Figures 4(a-c) compare the LB and DSMC results for Π with respect to T_w for $1 \text{ K} \leq T_w \leq 3000 \text{ K}$, at $\delta = 10, 1$ and 0.1 . It can be seen that Π presents only slight variations with respect to T_w at fixed values of δ and the LB results generally follow the same trend as the DSMC results. The general shape of these variations are similar to those of the associated viscosity index ω , shown in Fig. 1(b). The agreement between the LB and DSMC results deteriorates as δ is decreased, however the relative error $\Pi_{\text{LB}} / \Pi_{\text{DSMC}} - 1$ always remains below 2.5%, being largest surprisingly at $\delta \simeq 1$.

The simulation results presented in this section for $\delta = 1$ and 10 were obtained using the models $\text{HHLB}(6; 7) \times \text{HLB}(6; 7)$. As remarked in Refs. [6, 16], higher orders Q_x of the half-range Gauss-Hermite quadrature are required when $\delta \lesssim 1$ in order to get accurate solutions of the relaxation time model equation. For this reason, the results presented for $\delta = 0.1$ are obtained using the $\text{HHLB}(10; 16) \times \text{HLB}(6; 7)$ model. The values obtained for Π (4.1) using these models were within 0.1% of those obtained with the reference model $\text{HHLB}(10; 50) \times \text{HLB}(6; 7)$ on a grid employing $S = 48$ points. Note that also the values of Π , obtained with the DSMC method, have an error below 0.1% [14].

V. CONCLUSION

In this paper, we presented a comparison of lattice Boltzmann (LB) and direct simulation Monte Carlo (DSMC) results in the context of Couette flow between parallel plates for ^3He and ^4He gases at temperatures between 1 K and 3000 K. The LB implementation employs the half-range and full-range Gauss-Hermite quadratures on the x and y axes, respectively. The order $Q_y = 7$ of the full-range Gauss-Hermite quadrature is sufficient to obtain accurate results for all tested values of the rarefaction parameter δ . The quadrature order on the horizontal axis is taken to be $Q_x = 7$ when $\delta = 1$ and $\delta = 10$, while at $\delta = 0.1$, it is increased to $Q_x = 16$. The total number of velocities is $2Q_x Q_y = 98$ for $\delta = 1$ and $\delta = 10$, while at $\delta = 0.1$, 224 velocities are required in order to maintain good accuracy. The agreement obtained with the DSMC results is very good and the relative error in the off-diagonal component T_{xy} of the pressure tensor remains under 2.5%, even at $\delta = 0.1$. The use of the fifth order WENO scheme and of a third order TVD Runge-Kutta algorithm allows accurate results to be obtained using only 16 grid nodes on the right half of the channel, which are appropriately stretched towards the diffuse reflecting wall. While the discussion in this paper is limited to the Couette flow between parallel plates, we note that the LB models based on half-range quadratures can be employed also for flows in non-rectangular (curved) domains, e.g., when coupled with the vielbein approach,

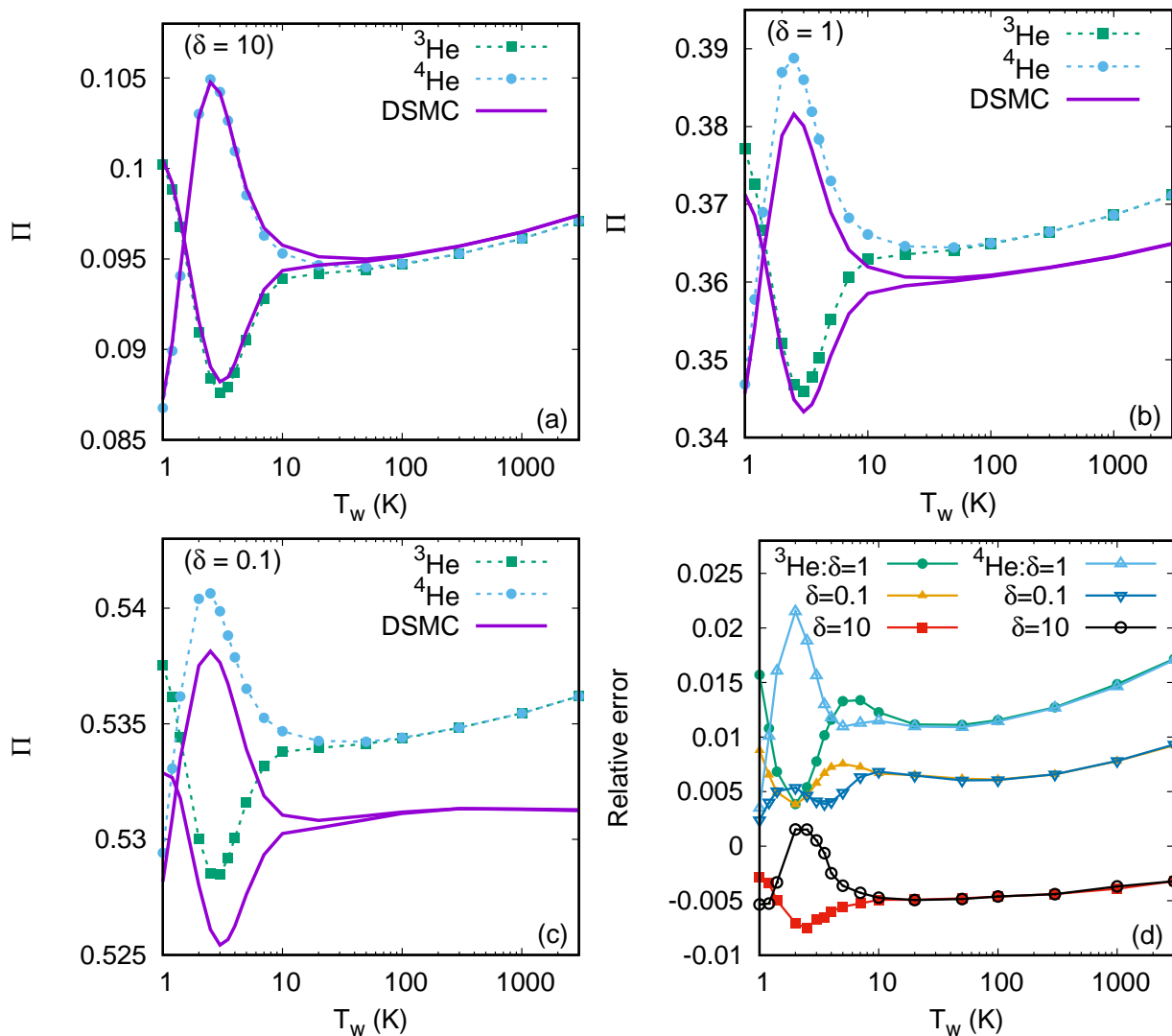


FIG. 4. (a-c) Dependence of Π (4.1) on the wall temperature T_w for both ^3He and ^4He , at $\delta = 10, 1$ and 0.1 . (d) Relative error $\Pi_{\text{LB}}/\Pi_{\text{DSMC}} - 1$ as a function of T_w for $\delta \in \{10, 1, 0.1\}$.

as discussed in Ref. [25].

VI. ACKNOWLEDGMENTS

V.E.A. was supported by a grant of the Romanian Ministry of Research and Innovation, CCCDI-UEFISCDI, project number PN-III-P1-1.2-PCCDI-2017-0371, within PNCIDI III. F.Sh. is supported by CNPq (Brazil), grant 303697/2014-8.

-
- [1] P. L. Bhatnagar, E. P. Gross, M. Krook, *Phys. Rev.* **94**, 511–525 (1954).
 - [2] E. M. Shakhov, *Fluid Dyn.* **3**, 95–96 (1968).
 - [3] F. Sharipov, *Rarefied gas dynamics* (Wiley-VCH, 2016).
 - [4] Z. Guo, K. Xu, and R. Wang, *Phys. Rev. E* **88**, 033305 (2013).
 - [5] A. Xu, G. Zhang, Y. Zhang, “Discrete Boltzmann modeling of compressible flows”, in *Kinetic Theory*, edited by G. Z. Kyzas and A. C. Mitropoulos (IntechOpen, Washington, DC, 2018), pp. 450–458.
 - [6] V. E. Ambruş and V. Sofonea, *J. Comput. Phys.* **316**, 760–788 (2016).
 - [7] W. P. Yudistiawan, S. K. Kwak, D. V. Patil, and S. Ansumali, *Phys. Rev. E* **82**, 046701 (2010).

- [8] V. E. Ambruş and V. Sofonea, *Phys. Rev. E* **86**, 016708 (2012).
- [9] J. Meng, Y. Zhang, N. G. Hadjiconstantinou, G. A. Radtke, and X. Shan, *J. Fluid Mech.* **718**, 347–370 (2013).
- [10] B. Piaud, S. Blanco, R. Fournier, V. E. Ambruş and V. Sofonea, *Int. J. Mod. Phys. C* **25**, 1340016 (2014).
- [11] V. E. Ambruş and V. Sofonea, *J. Comput. Sci.* **17**, 403–417 (2016).
- [12] E. P. Gross, E. A. Jackson, and S. Ziering, *Ann. Phys.* **1**, 141–167 (1957).
- [13] S. Takata, H. Funagane, *J. Fluid Mech.* **717**, 30–47 (2013).
- [14] F. Sharipov, *Physica A* **508**, 797–805 (2018).
- [15] W. Cencek, M. Przybytek, J. Komasa, J. B. Mehl, B. Jeziorski, and K. Szalewicz, *J. Chem. Phys.* **136**, 224303 (2012).
- [16] V. E. Ambruş and V. Sofonea, *Phys. Rev. E* **98**, 063311 (2018).
- [17] Z.-H. Li, H.-X. Zhang, *J. Comput. Phys.* **193**, 708–738 (2004).
- [18] J. Meng, L. Wu, J. M. Reese, Y. Zhang, *J. Comput. Phys.* **251**, 383–395 (2013).
- [19] L. Gibelli, *Phys. Fluids* **24**, 022001 (2012).
- [20] F. B. Hildebrand, *Introduction to Numerical Analysis*, Second edition (Dover Publications, 1987).
- [21] B. Shizgal, *Spectral Methods in Chemistry and Physics: Applications to Kinetic Theory and Quantum Mechanics (Scientific Computation)* (Springer, 2015).
- [22] C. W. Shu and S. Osher, *J. Comput. Phys.* **77**, 439–471 (1988).
- [23] G. S. Jiang and C. W. Shu, *J. Comput. Phys.* **126**, 202–228 (1996).
- [24] R. Mei and W. Shyy, *J. Comput. Phys.* **143**, 426–448 (1998).
- [25] S. Busuioc and V. E. Ambruş, *Phys. Rev. E*, *in press* (arXiv:1708.05944 [physics.flu-dyn]).